

Resonant enhanced diffusion in time dependent flow

P. Castiglione¹, A. Crisanti¹, A. Mazzino^{2,3},
M. Vergassola² and A. Vulpiani¹

¹ Dipartimento di Fisica, and Istituto Nazionale di Fisica della Materia,
Università “La Sapienza”, P.le A. Moro 2, 00185 Roma, Italy.

² CNRS, Observatoire de Nice, B.P. 4229, 06304 Nice Cedex 4, France.

³ Dipartimento di Fisica, and Istituto Nazionale di Fisica della Materia,
Università di Genova, Via Dodecaneso 33, 16146 Genova, Italy.

October 30, 2018

Abstract

Explicit examples of scalar enhanced diffusion due to resonances between different transport mechanisms are presented. Their signature is provided by the sharp and narrow peaks observed in the effective diffusivity coefficients and, in the absence of molecular diffusion, by anomalous transport. For the time-dependent flow considered here, resonances arise between their oscillations in time and either molecular diffusion or a mean flow. The effective diffusivities are calculated using multiscale techniques.

PACS number(s): 47.27Qb; 47.27-i.

1 Introduction

Passive scalar transport in a given velocity field is an issue of both theoretical and applicative relevance [1, 2]. The combination of molecular and advective effects can lead to rather subtle behaviors, even in the case of simple laminar flow. A rather complete theory has been developed for the dynamics at long times and large scales (macro-dynamics), using multiscale techniques [3]. For incompressible velocity fields the macrodynamics in the presence of scale separation is governed by an effective equation which is always

diffusive and transport is always enhanced [4]. A sufficient condition ensuring the presence of scale separation for three-dimensional incompressible flow is a vector potential finite variance, both for static and time-dependent flow [5, 6] (with similar conditions for other space dimensionalities). The small-scale velocity field properties emerge via the effective diffusivity second-order tensor. Its calculation is reduced to the solution of one auxiliary partial differential equation that can be efficiently solved numerically [7, 8] and variational principles have also been derived [9]. The effective diffusivities for generic flow depend on all the mechanisms of transport, e.g. on the advecting velocity field, on the molecular noise, on the presence and the strength of possible mean flow [7, 10]. Each process is characterized by its typical time-scales and, if the latter are properly tuned, their mutual interference can produce resonance effects. These lead to strong enhancement of transport, reflected in sharp and narrow peaks in the effective diffusivity. Our aim here is to present explicit examples of such resonance effects in simple time-dependent incompressible velocity fields. In Section 2 the source of resonance is the presence of a large-scale velocity field. For random parallel flow (Sec. 2.1), explicit analytic expressions for the effective diffusivities are obtained and they indeed display strong peaks for specific strengths of the large-scale velocity. In Section 2.2 the robustness of resonance effects to variations of the scale separation ratio between the large- and the small-scale velocity field components is investigated. Numerical simulations show that the effects persist even for moderate scale separations. Section 3 is devoted to a time-periodic $2D$ flow widely studied to mimic the transport in Rayleigh-Bénard system [11, 12]. The snapshots of the velocity field are made of closed lines. The synchronization between the circulation in the cells and their global oscillation provides however for a very efficient way of jumping from cell to cell. This mechanism, similar to stochastic resonance [13, 14], makes the curve of the effective diffusivity *vs* the frequency ω of oscillation of the flow very structured. In the limit where the molecular diffusion vanishes, anomalous superdiffusion takes place for narrow windows of values of ω around the peaks. The anomaly is observed both in the second-order moment of particle dispersion and in the singular behavior of the effective diffusivity at high Péclet numbers. In Section 4 we study a $2D$ system consisting of the superposition of steady coherent structures and a random incoherent field with a typical correlation time τ . The resonance occurs now when the sweeping time of the coherent structure is close to τ . Conclusions are reserved for the final Section 5.

2 Parallel flow with a large scale velocity field

The passive scalar field $\theta(\mathbf{x}, t)$ obeys (see Ref. [15]) the equation :

$$\partial_t \theta(\mathbf{x}, t) + (\mathbf{v} \cdot \nabla) \theta(\mathbf{x}, t) = D_0 \Delta \theta(\mathbf{x}, t). \quad (1)$$

The velocity $\mathbf{v}(\mathbf{x}, t)$ is here assumed to be incompressible and given by the sum of two terms, \mathbf{u} and \mathbf{U} . The first is periodic both in space (in a cell of size l) and in time (the technique can be extended with some modifications to handle the case of random, homogeneous and stationary velocity fields). The second is the large-scale component of \mathbf{v} , varying on a typical scale L . It is assumed that $l/L = \epsilon \ll 1$, where ϵ is the parameter controlling the scale separation.

We are interested in the dynamics of the field $\theta(\mathbf{x}, t)$ on large scales $\sim O(L)$, comparable to those of \mathbf{U} . In the spirit of multiscale methods [3], slow variables $\mathbf{X} = \epsilon\mathbf{x}$, $T = \epsilon^2 t$ and $\tau_\epsilon = \epsilon t$ are introduced in addition to the fast variables \mathbf{x} and t . The time variable τ_ϵ is needed to account for the advective effects generated by the presence of \mathbf{U} . The effective equation governing the dynamics at large scales of the field θ is [10]:

$$\partial_t \theta + \mathbf{U} \cdot \nabla \theta = \nabla_\alpha D_{\alpha\beta} \nabla_\beta \theta, \quad (2)$$

where the second-order eddy-diffusivity tensor is given by

$$D_{\alpha\beta}(\mathbf{X}, T) = \delta_{\alpha\beta} D_0 - \frac{1}{2} [\langle u_\alpha w_\beta \rangle + \langle u_\beta w_\alpha \rangle], \quad (3)$$

and the symbol $\langle \cdot \rangle$ denotes the average over the periodicities of the small-scale velocity field \mathbf{u} . The auxiliary field $\mathbf{w}(\mathbf{x}, t; \mathbf{X}, T)$ has vanishing average over the periodicities and satisfies the equation

$$\partial_t \mathbf{w} + [(\mathbf{u} + \mathbf{U}) \cdot \partial] \mathbf{w} - D_0 \partial^2 \mathbf{w} = -\mathbf{u} \quad . \quad (4)$$

2.1 A solvable case

A well-known situation where the effective diffusivities can be calculated analytically is the one of parallel flow. Let us consider in detail the case of three-dimensional random parallel flow in the presence of a large scale advecting velocity field $\mathbf{U}(\mathbf{X}, T)$:

$$\mathbf{u}(\mathbf{x}, t) = (u(y, z, t), 0, 0) ; \quad \mathbf{U}(\mathbf{X}, T) = (0, U(X, Z, T), 0). \quad (5)$$

The field $\mathbf{u}(\mathbf{x}, t)$ is random, homogeneous and stationary. The specific dependence on the spatial variables makes the fields automatically incompressible. The above decomposition is standard in the framework of mesoscale meteorology [16]. Its physical meaning is that small-scale eddies remain stationary while slow modifications of the large scale component occur. This is quite a common feature in geophysics, e.g. in the planetary boundary layer [17], where the airflow in the thin atmospheric layer near the ground is strongly driven by sink/source forcing terms arising from the bottom boundary.

The first component of the equation (4), the only one for which the r.h.s. does not vanish, can be easily solved in Fourier space and its solution reads:

$$\hat{w}_1(\mathbf{k}, \omega; \mathbf{X}, T) = \frac{-\hat{u}(\mathbf{k}, \omega)}{i\omega + k^2 D_0 + i\mathbf{U} \cdot \mathbf{k}} = -\hat{u}(\mathbf{k}, \omega) \hat{G}(\mathbf{k}, \omega; \mathbf{X}, T) \quad , \quad (6)$$

where the advection–diffusion propagator $\hat{G}(\mathbf{k}, \omega; \mathbf{X}, T)$ is defined as:

$$\hat{G}(\mathbf{k}, \omega; \mathbf{X}, T) = \frac{1}{i\omega + k^2 D_0 + i\mathbf{U} \cdot \mathbf{k}} = \int_0^{+\infty} e^{-[i\omega + k^2 D_0 + i\mathbf{U} \cdot \mathbf{k}] \alpha} d\alpha \quad .$$

It follows from (3) that the only non–vanishing elements of the eddy–diffusivity tensor are diagonal and:

$$D_{xx}(\mathbf{X}, T) = D_0 + \int_0^\infty S(t) \int \hat{E}(\mathbf{k}) e^{-[k^2 D_0 + i\mathbf{U} \cdot \mathbf{k}] t} dt d\mathbf{k}; \quad D_{yy} = D_{zz} = D_0 \quad , \quad (7)$$

We have for simplicity assumed the separability $\hat{E}(\mathbf{k}, \omega) = \hat{E}(\mathbf{k}) \hat{S}(\omega)$, where $\hat{E}(\mathbf{k})$ and $\hat{S}(\omega)$ are the spectra of the spatial and the temporal part of the correlation function of \mathbf{u} .

The simple analytic expression (7) can be used to address the question of interest in this paper, i.e., whether it is possible to have a resonance between the oscillation frequencies induced by U and the small–scale velocity field. We shall assume for simplicity U to be independent of both \mathbf{X} and \mathbf{T} and the following temporal part of the velocity correlation function:

$$S(t) = e^{-|t|/\tau} \cos(\omega t) \quad . \quad (8)$$

Substituting (8) into (7) and performing a simple integration, the latter takes the form:

$$D = D_0 + \tau_0 \int_0^\infty \hat{E}(k) R(k) dk. \quad (9)$$

Here, the function $R(k)$ is

$$R(k) = \frac{\left(\frac{1+\omega^2\tau^2}{1+k^2 D_0 \tau} \right) \left[1 + \left(\frac{\omega\tau}{1+k^2 D_0 \tau} \right)^2 + \left(\frac{U\tau k}{1+k^2 D_0 \tau} \right)^2 \right]}{\left[1 + \left(\frac{\omega\tau}{1+k^2 D_0 \tau} \right)^2 + \left(\frac{Uk\tau}{1+D_0 k^2 \tau} \right)^2 \right]^2 - 4 \left[\frac{\omega U k \tau^2}{(1+D_0 k^2 \tau)^2} \right]^2} \quad (10)$$

and τ_0 is the correlation time of turbulence:

$$\tau_0 = \int_0^\infty S(t) dt = \frac{\tau}{1 + \omega^2 \tau^2} \quad . \quad (11)$$

Note that $R(k) \rightarrow 1$ when both $U \rightarrow 0$ and $D_0 \rightarrow 0$. In the latter case $D = u_0^2 \tau_0$, the well known result valid for velocity fields δ –correlated in time (see, e.g., Ref. [8]). It

follows from (9) that the combined effect of D_0 and U is to modify the correlation time of turbulence, producing an effective correlation time $\tau_{eff} = \tau_0 R(k)$, which depends on the wavenumber k . It is precisely such a dependence on k that makes it possible to have resonances. Let us indeed consider (10) for a vanishing value of D_0 . It is easy to verify that, for $\omega\tau > 1/\sqrt{3}$, $R(k)$ has a peak for

$$U^{res} = \frac{1}{k\tau} \sqrt{-\omega^2\tau^2 - 1 + 2\omega\tau\sqrt{\omega^2\tau^2 + 1}}. \quad (12)$$

In the limit $\omega\tau \gg 1$, the previous expression reduces to: $U^{res} = \frac{\omega}{k}$. Note that $R(k)$ crosses the unit value for $\omega\tau > 1/\sqrt{3}$. The regime $R(k) > 1$ corresponds to constructive interference between the turbulent motion and the slow-varying one [18]. Destructive interference takes place, on the contrary, for $\omega\tau \leq 1/\sqrt{3}$ where $R(k)$ monotonically decreases from 1 ($U = 0$) to zero (large U). The effective diffusivity for small-scale flows with a single wavenumber \mathbf{k}_0 , attains at the maximum the value

$$D^{res} = u_0^2\tau_0 \frac{(1 + \omega^2\tau^2)(1 + 2\omega^2\tau^2)}{1 + 4\omega^2\tau^2}. \quad (13)$$

When $\omega\tau \gg 1$ (and the velocity U is ‘synchronized’ with the oscillating velocity field ($U^{res} = \omega/k_0$)), the previous expression reduces to $u_0^2\tau_0 \frac{\omega^2\tau^2}{2}$. For $U \gg \omega/k_0$, the effective diffusivity D goes to zero quadratically, as $D = u_0^2\tau_0 \left(\frac{\omega}{k_0U}\right)^2$.

The final result is that for a random parallel flow periodic in a box of size L ($k_0 = 2\pi/L$) and $\omega\tau \gg 1$, the peaks of the effective diffusivity D occur for

$$U_n^{res} = \frac{\omega}{k_0 n} \quad n = 1, 2, \dots, \quad (14)$$

with values given, for large U , by :

$$D_n^{res} \sim \hat{E}(k_0 n)\tau_0 \frac{\omega^2\tau^2}{2}. \quad (15)$$

The behavior of D as a function of U , obtained evaluating numerically the integral (9), is shown in Fig. 1 for a Kolmogorov spectrum $\hat{E}(k) \propto k^{-5/3}$, and for three different values of $\omega\tau \geq 1/\sqrt{3}$. Peaks of enhanced diffusion are evident for values of U given by (14). Note that for $\omega\tau = 40$, the first five peaks of D (from right to left) are close to the values given by the expression (15).

The role of a non-vanishing molecular diffusivity D_0 is to reduce the height of the peaks. This point is shown in Fig. 2, where the behavior of $D/(u_0^2\tau_0)$ is plotted as a function of $Uk_0\tau$, for $\omega\tau = 40$ and for three different values of D_0 . As we shall see in the following, these features hold also for more general flows than those considered in this section.

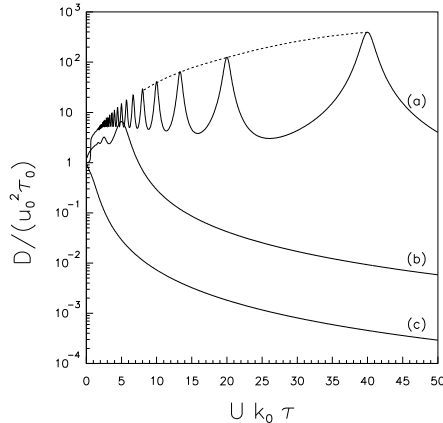


Figure 1: The eddy-diffusivity $D/(u_0^2 \tau_0)$ vs the mean flow strength $U k_0 \tau$. The curve is obtained by numerical integration of (9) for $D_0 = 0$, $\hat{E}(k) \propto k^{-5/3}$, temporal correlation function $S(t) = e^{-|t|/\tau} \cos(\omega t)$ and Strouhal number $S \equiv u_0 \tau_0 k_0 \sim 1$. The three curves correspond to (a): $\omega \tau = 40$; (b): $\omega \tau = 5$; (c): $\omega \tau = 1/\sqrt{3}$. The dashed line joins the peaks of D given by the expression (15) for $n = 1, 2, \dots, 5$.

It is finally worth noting that parallel flow permit to present yet another simple example of resonance. Considering indeed the expression (9) for vanishing values of U , it is easy to verify that for

$$D_0 = \frac{\omega \tau - 1}{k^2 \tau} \sim \frac{\omega}{k^2} \quad (16)$$

peaks of D occur. This corresponds to a synchronization between the characteristic viscous frequency $k^2 D_0$ of the random molecular noise and the frequency ω of the oscillatory velocity field.

2.2 Parallel flow with moderate scale separations

The aim here is to show that the resonant enhanced diffusion previously discussed also appears when only moderate scale separation factors are present. As in (1), consider indeed the velocity field $\mathbf{v} = \mathbf{u} + \mathbf{U}$ with \mathbf{u} parallel to the x axis

$$\mathbf{u} = (u_1 \cos(k_1 y + \omega_1 t), 0, 0) \quad (17)$$

and \mathbf{U} parallel to the y axis

$$\mathbf{U} = (0, u_2 \cos(k_2 x + \omega_2 t), 0) \quad (18)$$

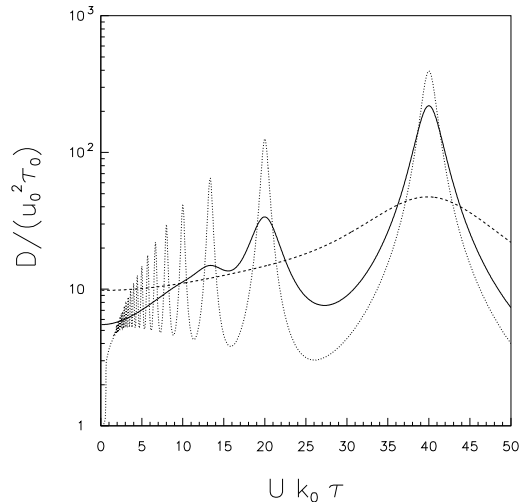


Figure 2: The same as in Fig. 1, but the behavior of $D/(u_0^2 \tau_0)$ is now plotted for three different values of D_0 and $\omega \tau = 40$. Dotted line: $D_0 = 0$; full line: $D_0/(u_0^2 \tau_0) = 5 \times 10^{-4}$; dashed line: $D_0/(u_0^2 \tau_0) = 5 \times 10^{-3}$. Note that the larger is D_0 , the broader are the peaks.

and $k_1 > k_2$. The situation $k_1 \gg k_2$ corresponds to the scale-separated case previously considered. Here, we shall assume $k_1 = 2.5 k_2$ (and $u_1 = u_2$) and we shall be interested in the dynamics at scales much larger than $1/k_2$. The two components of the velocity field \mathbf{v} have moderate scale separation and affect transport on equal footing. The velocity \mathbf{v} not being a parallel flow, analytical expressions for the effective diffusivities D_{ij} are not available anymore. We had then to solve numerically the standard auxiliary equation arising from multiscale methods (see, e.g., Ref. [8]). The equation is solved by using a pseudo-spectral method [21] in the basic periodicity cell with a grid mesh of 64×64 points. De-aliasing has been obtained by a proper circular truncation which ensures better isotropy of numerical treatment. Time marching has been performed using a leap-frog scheme mixed with a predictor-corrector scheme (see Ref. [22]) at regular intervals.

To enlighten the resonant diffusion enhancement, ω_1 is fixed and the D_{ij} behavior as a function of ω_2 is investigated. Results are reported in Figs. 3 and 4, where $D_{ii}/(u_0^2 \tau_1)$ vs $4\omega_2/\omega_1$ is presented for different values of D_0 . Here, $u_0^2 = u_1^2 + u_2^2$ and $\tau_1 = 2\pi/\omega_1$ is the oscillation period of the small-scale component. Results clearly exhibits resonance peaks for $\omega_2 = \omega_1$, $\omega_2 = \omega_1/2$, $\omega_2 \sim \omega_{sw}$ and $\omega_2 \sim 2\omega_{sw}$, where the frequency ω_{sw} is defined as:

$$\omega_{sw} = \frac{2\pi}{T_{sw}} \quad \text{with} \quad T_{sw} = \frac{L}{u_0}$$

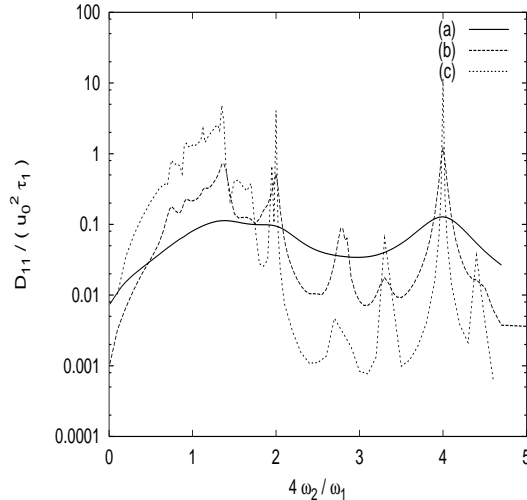


Figure 3: The non-dimensional eddy-diffusivity $D_{11}/(u_0^2 \tau_1)$ vs the non-dimensional frequency $4\omega_2/\omega_1$, for different values of $D_0/(u_0^2 \tau_1)$. The cases (a), (b) and (c) correspond to $D_0/(u_0^2 \tau_1) = 3 \times 10^{-3}$, $D_0/(u_0^2 \tau_1) = 3 \times 10^{-4}$ and $D_0/(u_0^2 \tau_1) = 3 \times 10^{-5}$, respectively.

and $4\omega_{sw}/\omega_1 = \sqrt{2}$. There are other peaks for $\omega < \omega_{sw}$, corresponding to submultiples of ω_1 and ω_{sw} .

Note in Fig. 4 that D_{22} increases for $\omega_2 \rightarrow 0$. This is qualitatively understood as follows : for small ω_2 , the velocity field is essentially a stationary shear flow in the y direction superimposed to a rapidly changing small-scale component. The picture is rather close to the Taylor mechanism for the longitudinal diffusion in the shear flow, which is well known to lead to a $1/D_0$ behavior for D_{22} [23].

3 Diffusion in time-periodic Rayleigh-Benard convection

Let us consider the two-dimensional velocity field defined by the following stream function :

$$\psi(x, y, t) = \psi_0 \sin(x + B \sin \omega t) \sin y \quad . \quad (19)$$

This flow [11, 12] is a simple model for transport in time-periodic Rayleigh-Bénard convection. The stream function (19) describes single-mode, two-dimensional convection with rigid boundary condition. The even oscillatory instability [19] is accounted for by the

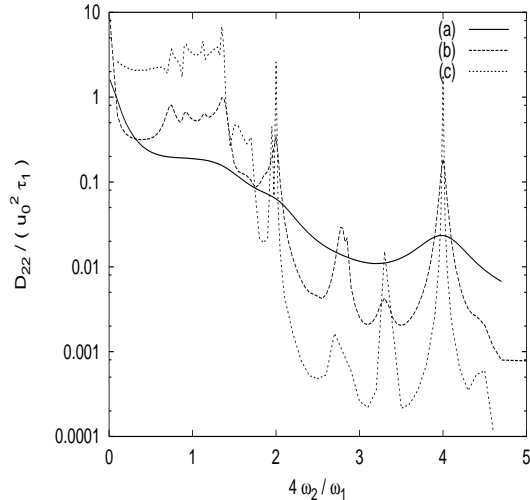


Figure 4: The non dimensional eddy-diffusivity $D_{22}/(u_0^2\tau_1)$ vs the non dimensional frequency $4\omega_2/\omega_1$, for different values of $D_0/(u_0^2\tau_1)$. The cases (a), (b) and (c) correspond to $D_0/(u_0^2\tau_1) = 3 \times 10^{-3}$, $D_0/(u_0^2\tau_1) = 3 \times 10^{-4}$ and $D_0/(u_0^2\tau_1) = 3 \times 10^{-5}$, respectively.

term $B \sin \omega t$, representing the lateral oscillation of the roll. In Ref. [12], a quantitative comparison of the behavior in this flow with the experimental data has shown that the basic mechanisms of convective transport are well captured by the expression (19).

For a fixed ωt , the oscillation frequency of a Lagrangian particle close to the center of the periodic cell is of the order of ψ_0 . The periodicity of the cell is $L \equiv 2\pi$ and the dimensionless parameter controlling the dynamics is $\epsilon = \omega L^2/\psi_0$. The two limiting regimes $\epsilon \ll 1$ and $\epsilon \gg 1$ have been investigated in Ref. [20] to obtain the expressions of the diffusion coefficients in the limit of zero molecular diffusivity. Here, we shall concentrate on the behavior for $\epsilon \sim 1$. It is indeed precisely in this region that a synchronization between the characteristic frequencies $O(\psi_0)$ and $O(\omega)$ can take place. In all the cases reported here, a resolution 512×512 has been used, which is found adequate for molecular diffusivities $D_0/\psi_0 \geq 5 \times 10^{-4}$. The system evolution has been computed up to times $500 L^2/\psi_0$, with a time step $\Delta t = 10^{-2} L^2/\psi_0$.

For small enough (or vanishing) numerical diffusivities, the numerical integration of the partial differential equation (4) is clearly subject to instabilities. To evaluate the eddy-diffusivities, it is then more convenient to integrate the equation $d_t \mathbf{x} = \mathbf{v}$ using a second-order Runge-Kutta scheme and then performing a linear fit of $\langle [x(t) - x(0)]^2 \rangle$ vs t , to obtain the diffusion coefficient. The averages are made over different realizations

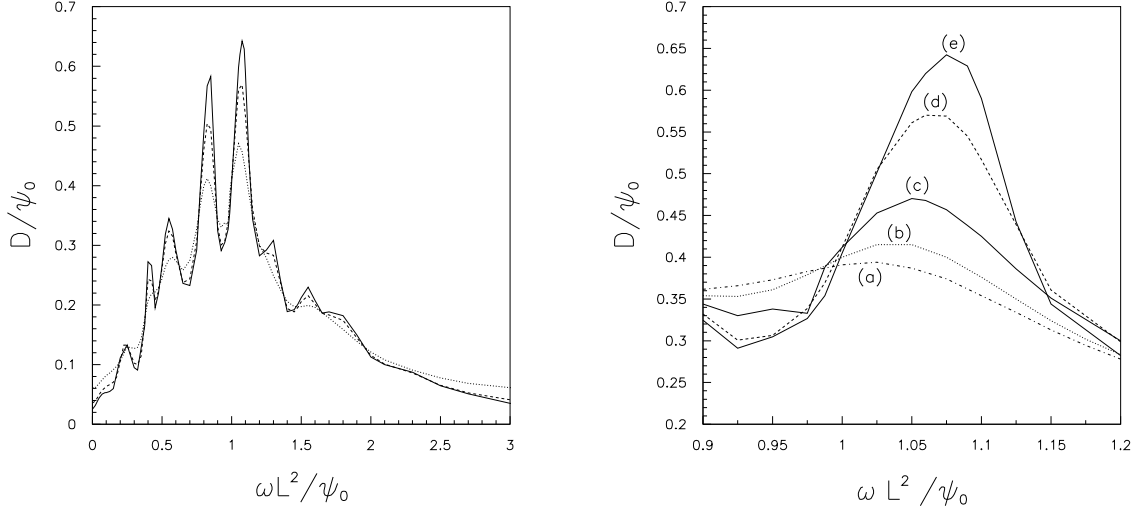


Figure 5: The turbulent diffusivity D/ψ_0 vs the frequency $\omega L^2/\psi_0$ for different values of the molecular diffusivity D_0/ψ_0 . On the left: $D_0/\psi_0 = 3 \times 10^{-3}$ (dotted line); $D_0/\psi_0 = 1 \times 10^{-3}$ (dashed line); $D_0/\psi_0 = 5 \times 10^{-4}$ (full line). On the right: $D_0/\psi_0 = 1 \times 10^{-2}$ (a); $D_0/\psi_0 = 6 \times 10^{-3}$ (b); $D_0/\psi_0 = 3 \times 10^{-3}$ (c); $D_0/\psi_0 = 1 \times 10^{-3}$ (d); $D_0/\psi_0 = 5 \times 10^{-4}$ (e).

and are performed by uniformly distributing 10^6 particles in the basic periodic cell. The system evolution has been computed up to times $10^4 L^2/\psi_0$. Numerical schemes have been tested both for vanishing values of ω and for large Péclet number. Asymptotic solutions for the effective diffusivity are indeed available in these limits (see Eq. (27) in Ref. [24]). Measured diffusion coefficients agree with the theoretical values within errors of less than 1%.

The turbulent diffusivity (the x -component) vs the frequency $\omega L^2/\psi_0$ is shown in Fig. 5 for different values of D_0/ψ_0 . A few comments are in order. First, the turbulent diffusivity shows maxima which seems similar to those observed for stochastic resonance [13, 14]. Here, the resonance is between the lateral roll oscillation frequency and the characteristic frequencies of the scalar field motion. Second, the effect of D_0 on the shape of the peaks is twofold: similarly to the case of the parallel flow, the smaller is D_0 , the sharper are the peaks. Furthermore, from the expanded view of Fig. 5 (on the right), it appears that variations of D_0 also cause a shifting of maxima positions.

For $D_0 \rightarrow 0$, the peak shown in Fig. 5 moves toward $\omega L^2/\psi_0 \sim 1.1$ and the transport becomes superdiffusive at $D_0 = 0$, i.e. the mean-squared displacement is superlinear:

$$\langle [x(t) - x(0)]^2 \rangle \propto t^\alpha \quad \text{with} \quad \alpha > 1 \quad . \quad (20)$$

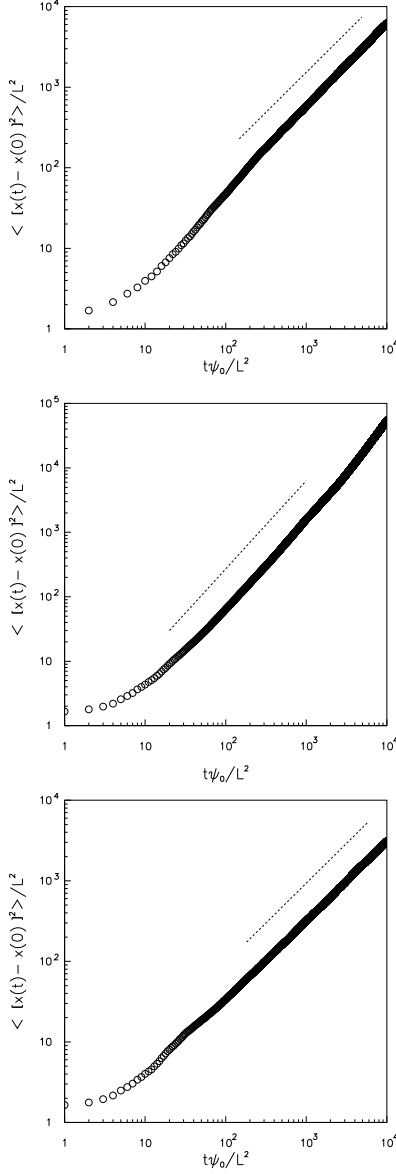


Figure 6: The mean-squared displacement *vs* the time for the flow (19) with $D_0 = 0$ (in a log-log scale). From above to below: $\omega L^2 / \psi_0 = 1.075$, $\omega L^2 / \psi_0 = 1.1$ and $\omega L^2 / \psi_0 = 1.15$. Dashed lines have slopes 1, 1.4 and 1, respectively.

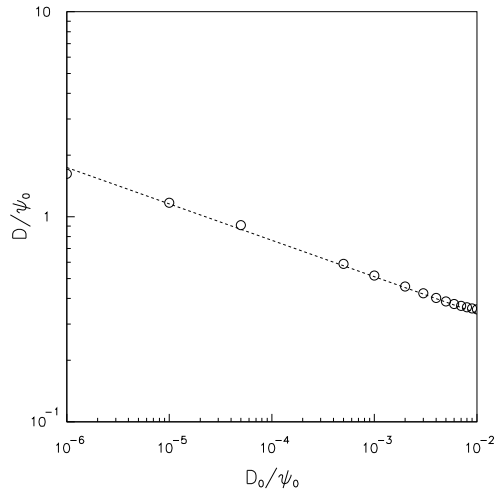


Figure 7: The diffusion coefficient D as a function of D_0 at $\omega L^2/\psi_0 = 1.1$ (in a log-log scale). The slope of the dashed line is $-\beta \sim 0.18$.

The range of $\omega L^2/\psi_0$ values where the process is superdiffusive turns out to be very narrow: for $\omega L^2/\psi_0 = 1.1$ the mean-squared displacement behavior is given by (20) with exponent $\alpha \sim 1.4$; both for $\omega L^2/\psi_0 = 1.075$ and $\omega L^2/\psi_0 = 1.15$ the diffusion process is standard (i.e., $\alpha = 1$). This point is illustrated in Fig. 6, where the mean-squared displacement as a function of the time is shown in a log-log plot for : $\omega L^2/\psi_0 = 1.075$, $\omega L^2/\psi_0 = 1.1$ and $\omega L^2/\psi_0 = 1.15$.

A more careful test of the anomalous diffusion at $D_0 = 0$ consists in computing the diffusion coefficient D as function of D_0 . As suggested in Ref. [8], in the presence of genuine anomalous diffusion, the effective diffusivity must diverge and it is expected that $D \sim D_0^{-\beta}$ with $\beta > 0$. The curve D versus D_0 at $\omega L^2/\psi_0 = 1.1$ is shown in Fig. 7. The data are well fitted by a straight line with slope $\beta \sim 0.18$, confirming the presence of anomalous diffusion at $D_0 = 0$.

4 Enhanced diffusion in the presence of coherent structures

We shall consider now the case where the two-dimensional large-scale component \mathbf{U} consists of a coherent structure. The small-scale part \mathbf{u} is random. Specifically, $\mathbf{u} = (u_1, u_2)$,

where the u_i 's are homogeneous, isotropic and stationary Gaussian random processes. Their Fourier transforms \hat{u}_i have zero mean and correlation functions :

$$\langle \hat{u}_i(\mathbf{k}, t) \hat{u}_j(\mathbf{k}', t') \rangle = (2\pi)^2 \delta(\mathbf{k} + \mathbf{k}') \hat{R}_{ij}(\mathbf{k}) T(\mathbf{k}, t - t') \quad (21)$$

where

$$\hat{R}_{ij}(\mathbf{k}) = (\delta_{ij} k^2 - k_i k_j) f(k) \quad \text{and} \quad T(\mathbf{k}, t - t') = e^{-\frac{|t-t'|}{\tau(k)}}.$$

The $f(k)$ function is related to the field energy spectrum $E(k)$ as follows:

$$E(k) = \frac{1}{2\pi} k^3 f(k).$$

The following expressions for $E(k)$ and $\tau(k)$ have been considered :

$$E(k) = \begin{cases} A k^3 & k \in [0, k_m^I] \\ B k^{-\frac{5}{3}} & k \in [k_m^I, k_M^I] \\ C e^{-k} & k > k_M^I \end{cases} \quad (22)$$

and

$$\tau(k) = \begin{cases} D k^{-3} & k \in [0, k_m^I] \\ F k^{-\frac{2}{3}} & k \in [k_m^I, k_M^I] \\ G k^{-\frac{3}{2}} e^{\frac{k}{2}} & k > k_M^I \end{cases} \quad (23)$$

where the constants A , C and D , G are chosen to ensure the continuity of $E(k)$ and $\tau(k)$ in k_m^I and k_M^I , respectively. The expression for $\tau(k)$ is meant to mimic 3D turbulence, neglecting intermittency and correlations between phases. The $\hat{u}_i(\mathbf{k}, t)$ can be easily generated by a linear Langevin equation. The coherent large-scale component has the cellular structure

$$\mathbf{U} = U (\cos y, \cos x) \quad (24)$$

characterized by the typical Lagrangian time $T_c = \pi/(\sqrt{2}U)$. From the isotropy of the field it follows $D_{11} = D_{22} \equiv D$. In Fig. 8 the diffusion coefficient $D/(u_0^2 \tau_1)$ is shown as a function of T_c/τ_1 , where $\tau_1 = \tau(k_m^I)$ is a characteristic time scale of the random field and $u_0^2 = \int dk E(k)$.

The above results have been obtained performing direct numerical simulations of the auxiliary equation (4) (now $\mathbf{U} = 0$ and \mathbf{u} has the spectrum defined by (22)) by using a pseudo-spectral method over the periodic box $2\pi \times 2\pi$ with a resolution 64×64 .

It is well evident the presence of a peak for $T_c/\tau_1 \sim 7$ and $D_0/(u_0^2 \tau_1) = 3.9 \times 10^{-4}$, whose value is $D/(u_0^2 \tau_1) \sim 0.86$. The fact that the peak does not appear for T_c/τ_1 of order unity is most likely due just to the freedom in the definition of the characteristic times T_c and τ_1 . On the contrary, it is important to note that the value of the peak is much larger

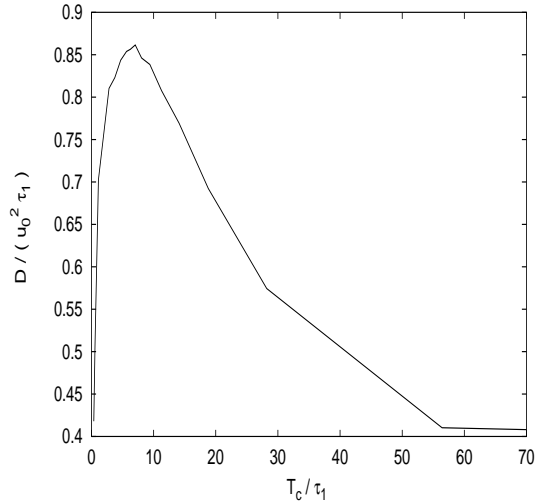


Figure 8: The non dimensional eddy-diffusivity $D/(u_0^2 \tau_1)$ vs the non dimensional Lagrangian time T_c/τ_1 for $D_0/(u_0^2 \tau_1) = 3.9 \times 10^{-4}$ and $k_M^I/k_m^I = 4.5$.

than the one occurring when either the random field or the coherent structure are absent. The value $D/(u_0^2 \tau_1) \sim 0.86$ has in fact to be compared with 0.07 and 0.32, respectively.

Unlike the resonance in the Reyleigh-Bénard convection, the synchronization mechanism produces here a broad peak. This is not surprising as in the present case the random field has a wide spectrum of characteristic times.

5 Conclusions

Multiscale techniques have been used to present a series of explicit examples of strong diffusion enhancement due to resonance effects between different transport mechanisms. The effects appear already from the analytical expression of eddy-diffusivity for random flows with a large scale mean flow component, are robust to a reduction of the scale separation and they are also observed in convective transport and when coherent structures are present on the large scales. For vanishing molecular diffusivities and for specific values of the control parameters, the enhanced diffusion might turn into anomalous superdiffusion. Let us finally stress in which respect the resonant enhanced diffusion effects discussed in this paper differ from other known mechanisms to produce strong transport. For Taylor longitudinal diffusion in shear flow, open streamlines producing large effective diffusivities are for example present in the snapshots of the velocity field itself. For the convective

flow in Section 3, snapshots of the velocity field are made at every time of closed cells. Open streamlines, and more generally enhanced transport, have a dynamical origin and require a temporal synchronization between different transport mechanisms.

Acknowledgments

We thank the “Meteo–Hydrological Center of Liguria Region” and the “Department of Structural and Geotechnical Engineering of the University of Genova” where part of the numerical analysis was done. AM is grateful to C.F. Ratto for very useful discussions and suggestions. AM was supported by the “Henry Poincaré” fellowship (Centre National de la Recherche Scientifique and Conseil Général des Alpes Maritimes) and by a fellowship “di Prosecurazione” (Università degli Studi di Genova). PC is grateful to the European Science Foundation for the TAO exchange grant. MV was supported by the GdR “Mécanique des Fluides Géophysiques et Astrophysiques”. PC, AC and AV were supported by INFM (PRA-TURBO).

References

- [1] H.K. Moffatt, *Rep. Prog. Phys.*, **46**, 621, (1983).
- [2] A. Crisanti, M. Falcioni, G. Paladin and A. Vulpiani, *Riv. Nuovo Cimento*, **14**, 1, (1991).
- [3] A. Bensoussan, J.-L. Lions and G. Papanicolaou, *Asymptotic Analysis for Periodic Structures* (North-Holland, Amsterdam, 1978).
- [4] D. Mc Laughlin, G.C. Papanicolaou and O. Pironneau, *SIAM Journal of Appl. Math.*, **45**, 780, (1985).
- [5] M. Avellaneda and A. Majda, *Commun. Math. Phys.*, **138**, 339, (1991).
- [6] M. Avellaneda and M. Vergassola, *Phys. Rev. E*, **52**, 3249, (1995).
- [7] A. Majda and R. McLaughlin, *Stud. Appl. Math.*, **89**, 245, (1993).
- [8] L. Biferale, A. Crisanti, M. Vergassola and A. Vulpiani, *Phys. Fluids*, **7**, 2725 (1995).
- [9] A. Fannjang and G.C. Papanicolau, *SIAM J. Appl. Math.*, **54**, 333, (1994).
- [10] A. Mazzino, *Phys. Rev. E*, **56**, 5500 (1997).
- [11] J.P. Gollub and T.H. Solomon, in *Proceedings of the Fritz Haber International Symposium*, ed. by I. Procaccia (Plenum, New York, 1988).
- [12] T.H. Solomon and J.P. Gollub, *Phys. Rev. A*, **38**, 6280 (1988).
- [13] R. Benzi, A. Sutera and A. Vulpiani, *J. Phys.*, **14**, L453 (1981).
- [14] R. Benzi, G. Parisi, A. Sutera and A. Vulpiani, *SIAM Journal Appl. Math.*, **43**, 565 (1983).
- [15] S. Chandrasekhar, *Rev. Mod. Phys.*, **15**, 1 (1943).
- [16] R. Pielke, *Mesoscale Meteorological Modeling* (Academic Press, Inc., Orlando, Florida, 1984).
- [17] Z. Sorbjan, *Structure of the Atmospheric Boundary Layer* (Englewood Cliffs, N.J., 1989).
- [18] A.Mazzino and M. Vergassola, *Europhys. Lett.*, **37**, 535 (1997).

- [19] R.M. Clever and Busse F.H., *J. Fluid Mech.*, **65**, 625 (1974).
- [20] A.A. Chernikov, A.I. Neishtadt, A.V. Rogal'sky and V.Z. Yakhnin, *Chaos*, **1**, 206 (1991).
- [21] D. Gottlieb and S.A. Orszag, *Numerical analysis of spectral methods*, SIAM, (Philadelphia, Pa., 1977).
- [22] G.I. Marchuk, *Methods of Numerical Mathematics*, (Springer-Verlag, 1975).
- [23] G.I. Taylor, *Proc. R. Soc. A*, **219**, 186, (1953) and *Proc. R. Soc. A*, **225**, 473, (1954).
- [24] M.N. Rosebluth, H.L. Berk, I. Doxas and W. Horton, *Phys. Fluids*, **30**, 2636 (1987).